


## Article

# Comprehensive Utilization of Fossil Energy: Fabrication of Fire-Retardant Building Materials from Waste Plastic

Zheng Wang, Long Geng, Jiateng Zhao, Wenyuan Qiao and Changhui Liu \* School of Low-Carbon Energy and Power Engineering, China University of Mining and Technology,  
Xuzhou 221116, China

\* Correspondence: liuch915@cumt.edu.cn

**Abstract:** As one of the most common fossil derivatives, plastics are widely used for their exceptional chemical stability, low density, and ease of processing. In recent years, there has been a significant increase in the production of waste plastics, coupled with a low recycling rate, resulting in serious environmental pollution. To enhance the use of waste plastics, this research synthesized flame-retardant materials from hypercrosslinked polystyrene with different molar fractions of flame retardants. Waste polystyrene foam was used as the raw material, while aniline, triphenylphosphine, and melamine were employed as flame-retardant additives. The flame-retardant additives were successfully doped into the porous skeleton structure of hypercrosslinked polystyrene through a chemical reaction or physical mixing to achieve in situ flame retardancy, and the materials were shaped by a phenolic resin prepolymer. Then, the samples were characterized in detail, and the results indicate that the addition of a flame retardant enhances the flame retardancy of the material. In addition, the material has excellent thermal insulation performance, with a minimum thermal conductivity of 0.04176 W/(m·K).

**Keywords:** waste plastic; recycle; material safety; excellent thermal insulation; flame retardant



**Citation:** Wang, Z.; Geng, L.; Zhao, J.; Qiao, W.; Liu, C. Comprehensive Utilization of Fossil Energy: Fabrication of Fire-Retardant Building Materials from Waste Plastic. *J. Compos. Sci.* **2024**, *8*, 266. <https://doi.org/10.3390/jcs8070266>

Academic Editor: Farshid Pahlevani

Received: 1 June 2024

Revised: 27 June 2024

Accepted: 8 July 2024

Published: 10 July 2024



**Copyright:** © 2024 by the authors. Licensee MDPI, Basel, Switzerland. This article is an open access article distributed under the terms and conditions of the Creative Commons Attribution (CC BY) license (<https://creativecommons.org/licenses/by/4.0/>).

## 1. Introduction

Plastics are derived from petroleum and are usually made by polymerizing monomers such as ethylene, propylene, and styrene. With the development of industry, plastics have become widely used in electrical, packaging, construction, medical, and other fields based on their excellent chemical stability, low density, and ease of processing, becoming an indispensable substance in modern life [1]. According to statistics, global plastic production has reached nearly 400 million tons. Most plastic waste ends up being incinerated or accumulating in landfills and the environment. Only 15–18% of plastic is recycled [2–6]. Based on this state of affairs, increasing the recycling of plastics is an important issue [3,7,8]. Notably, certain waste materials have been employed to substitute traditional petroleum-based flame retardants in polymeric materials [9–13]. Through the high-value recycling of plastics, fossil energy can be saved and environmental pollution reduced. And, it will help to reduce the need for oil and gas extraction, conserve limited fossil fuel resources, and reduce the pressure of climate change.

There are three main methods of converting waste polystyrene (PS) into flame-retardant materials. The first method involves coating the material's surface with flame-retardant materials to reduce heat and mass transfer between the gaseous medium and the condensed phase, thereby impeding flame propagation during a fire [14,15]. Li et al. [16] prepared biomass-based flame-retardant additives from renewable chitosan, melamine formaldehyde resin-coated ammonium polyphosphate, and organic montmorillonite, which were then blended into waterborne epoxy resin (WBEP) to produce waterborne flame-retardant coatings. The prepared flame-retardant WBEP coatings showed good water resistance and flame-retardant efficiency on wood substrates. However, the dispersion uniformity between the matrix and the coating, as well as the problem of poor interfacial

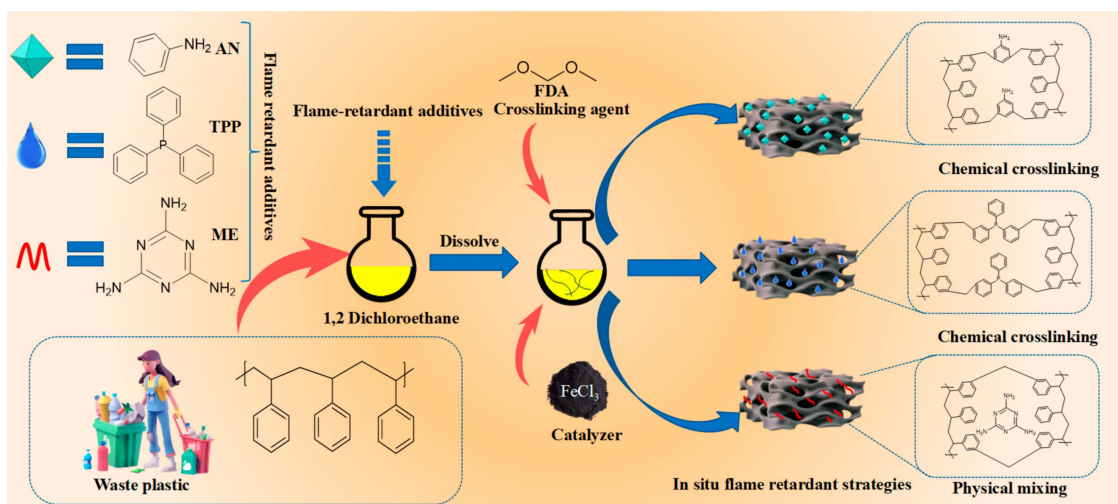
contact, has become an important factor restricting the development of flame-retardant coatings. For this reason, doping flame retardants has become another direction for the development of flame-retardant polystyrene. Presently, the primary categories of flame retardants include halogenated-based [17,18], phosphorus-based [19–21], intumescent [22], and nitrogen-based flame-retardant materials [23]. Halogenated flame retardants have been prohibited due to their detrimental impact on the environment and organisms [24]. Phosphorus flame retardants are both environmentally friendly and efficient; they tend to be less toxic than their organohalogen counterparts and are usually biodegradable to environmentally benign products; they are mainly divided into two types: organic phosphorus-based and inorganic phosphorus-based flame retardants [21,25,26]. Phosphorus flame retardants in different reaction zones can be divided into condensed-phase flame retardants and vapor-phase flame retardants, and in organic phosphorus flame retardants, the condensed phase plays an important flame-retardant role [27]. Intumescent flame retardants consist of an acid source, a carbon source, and a gas source, and when burned, a carbonaceous foam layer is generated on the surface, which serves as a thermal barrier to combustion [22,28,29]. Nitrogen-based flame retardants are susceptible to decomposition when exposed to heat, thus carrying away the heat generated during combustion and interrupting combustion [30,31].

At present, the methods of doping flame retardants are physical doping and chemical doping. Physical doping is mainly divided into in situ polymerization [32], melt mixing [33], and solution mixing [34]. For all approaches, a major challenge is the dispersion of carbon nanomaterials into polymer matrices. In this regard, chemical doping has received much attention due to its ability to dope flame retardants at fixed sites of the material to achieve in situ flame retardancy. Li et al. [35] developed a nitrogen–phosphorus synergistic flame-retardant plasticizer, named NPPF, by incorporating phosphate and chlorine flame retardants into the chemical structure of rubber seed oil, and they applied it to plasticized polyvinyl chloride (PVC). Material characterization results demonstrated that NPPF, with excellent solvent extraction resistance, could markedly enhance the limiting oxygen index and thermal stability of the plasticized PVC materials. Li et al. [36] employed graphene oxide (GO) as an in situ lamellar intumescent flame retardant (IFR) to produce flame-retardant polybutylene terephthalate materials with varying flame-retardant concentration gradients. The IFR was incorporated into the GO lamellar structure through a chemical reaction to achieve in situ flame retardancy, resulting in the significantly enhanced flame retardancy of the composites.

Currently, there are more studies on the recycling of waste PS by chemical methods. For example, Solís et al. [37] converted waste PS mixed with olivine through pyrolysis into activated carbon material and used it for CO<sub>2</sub> adsorption. Vijaya et al. [38] converted waste PS into electrode material for supercapacitors. Zhang et al. [39] pyrolyzed waste PS into porous carbon and used it to coat phase-change materials such as paraffin. There is one thing in common: the materials obtained are all porous materials. For the flame-retardant performance of materials, current research mainly focuses on the thermal stability, limiting oxygen index, and heat release rate of materials. It is worth paying attention to the fact that heat insulation is also a key index for evaluating the flame-retardant performance of a material. According to research, the larger the porosity of the material, the better its thermal insulation effect [40]. However, research on the conversion of used PS into flame-retardant materials by chemical methods is still rare. The research in this paper is the first trial of converting waste PS into porous media and doping it with a flame retardant to improve its thermal insulating properties while achieving an in situ flame retardant effect.

Based on the above situation and previous research experience on the high-value use of waste plastics [39,41,42], this paper develops a novel and simple method for the preparation of hypercrosslinked polystyrene (HCP) with high flame retardancy and excellent thermal insulating properties. Waste polystyrene foam was used as a raw material, and three flame-retardant additives were selected: aniline, triphenylphosphine, and melamine (Figure 1). Each material was successfully added to the porous structure of HCP through chemical

reactions or physical mixing, achieving an in situ flame-retardant effect, and the materials were shaped by a phenolic resin prepolymer. It is worth noting that this method not only greatly improves the flame-retardant effect of the material but also has a high thermal insulation performance, which provides an idea for the high-value recycling of discarded PS plastics, reduces its pollution of the environment, and has broad application prospects in the field of building energy saving.



**Figure 1.** Preparation process of HCP.

## 2. Materials and Methods

### 2.1. Materials

1,2-Dichloroethane (DCE) and  $\text{FeCl}_3$  were purchased from Shanghai Titan Technology Co. Ltd. (Shanghai, China). Aniline (AN) and triphenylphosphine (TPP) with Formaldehyde dimethyl acetal (FDA) were purchased from Aladdin Chemical Reagent Company (Shanghai, China). Melamine (ME) was purchased from Injury McLean Biochemistry Ltd. (Shanghai, China). The phenolic resin prepolymer (PRP) was purchased from Henan Platinum Run Casting Materials Co. (Zhengzhou, China). All reagents were used without further purification unless otherwise stated. Waste polystyrene foam was collected from daily life and had a density of about  $35.6 \text{ kg/m}^3$ .

### 2.2. Characterization

Fourier Transform Infrared Spectroscopy (FT-IR) spectra were recorded by using a VERTEX 70 (Bruker, Berlin, Germany) FT-IR as KBr discs. Thermogravimetric analysis (TGA) was carried out by heating from room temperature to  $800 \text{ }^\circ\text{C}$  at a rate of  $10 \text{ }^\circ\text{C}\cdot\text{min}^{-1}$  on a TA SDT Q600 instrument under a nitrogen atmosphere. X-ray polycrystalline diffractometer (XRD) patterns were recorded on a diffractometer (Smartlab, Aachen, Germany) with Ni-filtered  $\text{CuK}\alpha$  radiation ( $k = 0.154 \text{ nm}$ ) at a tube current of  $30 \text{ mA}$  and a generator voltage of  $40 \text{ kV}$ . Scanning was performed at a speed of  $8^\circ\cdot\text{min}^{-1}$ , from  $0$  to  $80^\circ$  of  $2\theta$ . The thermal conductivity of the samples was measured by using a thermal conductivity meter (Hot Disk 2500-OT, Göteborg, Sweden) based on the transient plane source method, and the testing temperature was adjusted and controlled by a water bath and an insulated chamber. Scanning electron microscope (SEM) images were recorded using an FEI Sirion 200 field-emission scanning electron microscope operating at  $10 \text{ kV}$ . Loss-on-ignition tests repeated 3 times, combustion tests repeated 5 times, and thermal conductivity tests repeated 5 times were performed.

### 2.3. Uncertainty Analysis

Uncertainty analysis is considered due to the uncertainty of the data acquisition devices. The temperature measurement error range for each measure is  $\pm 0.5 \text{ }^\circ\text{C}$ . The

thermal conductivity analyzer has an accuracy of  $\pm 3\%$  at a working temperature from  $-200$  to  $150$  °C.

#### 2.4. Synthesis of HCP

Waste PS foam (3 g) was dissolved in DCE (25 mL) and stirred for 1 h. After the waste PS was completely dissolved, the flame retardants AN, TPP, and ME were added according to the proportions shown in Table 1, and stirring was continued for 30 min. After the liquid was mixed well, FDA (3.2 mL) and FeCl<sub>3</sub> (15 mmol) were added in turn. The reaction temperature was set at 80 °C and stirring speed at 600 rpm for 20 h. Then, the solvent, DCE, was removed by evaporation using a rotary evaporator after the reaction was completed. Finally, the resulting product was dried in a vacuum oven at 80 °C for 12 h to obtain the final product HCP-x-y (x is the type of additive, and y is the molar ratio of the additive to waste polystyrene plastic). The specific experimental parameters are shown in Table 1.

**Table 1.** Preparation parameters of polystyrene-based plastic fireproofing material <sup>1</sup>.

Sample	PS (g)	AN (g)	TPP (g)	ME (g)	Mole Ratio
S1	3	-	-	-	-
S2	3	0.26	-	-	1: 10
S3	3	0.17	-	-	1: 15
S4	3	0.13	-	-	1: 20
S5	3	0.10	-	-	1: 25
S6	3	-	0.75	-	1: 10
S7	3	-	0.49	-	1: 15
S8	3	-	0.37	-	1: 20
S9	3	-	0.29	-	1: 25
S10	3	-	-	0.36	1: 10
S11	3	-	-	0.24	1: 15
S12	3	-	-	0.18	1: 20
S13	3	-	-	0.14	1: 25

<sup>1</sup> FeCl<sub>3</sub>: 15 mmol; DCE: 25 mL; FDA: 3.2 mL; reaction temperature: 80 °C.

#### 2.5. Synthesis of Phenolic Resin-Based HCP (PHCP)

Firstly, PHCP-x-y was obtained by mixing HCP-x-y with PRP at a mass ratio of 3:1, and 4 g of PHCP-x-y was placed in a rectangular mold (60 mm × 20 mm × 20 mm) and then thermally cured for 30 min at 150 °C in a thermostatic drying oven, and the resulting material was taken out and used for combustion testing. Then, 1 g of the prepared THCP-x-y was taken and placed in a tablet press, and the resulting circular tablet was placed in a constant-temperature drying oven for 30 min at 150 °C for heat curing. The resulting material was removed for thermal conductivity testing.

#### 2.6. Steps of Loss-on-Ignition Test

The specific operation steps are as follows: (1) Take 3 g of the sample and place it in a constant-temperature drying oven at 105 °C to dry for 1 h in order to remove external moisture from the material, and then stand by. (2) Measure the mass of the dry crucible with an analytical balance and record it as  $m_0$ . (3) Take 1 g of the sample and add it to the crucible, and measure the mass of the crucible and record it as  $m_1$ . (4) Put the crucible in a suitable position above the 150 mL capacity alcohol lamp (depending on the position of the flame), carry out the combustion, measure the mass of the crucible every 2 min, and record the data. (5) After the mass of the crucible is stabilized, remove and measure the mass of the crucible and record it as  $m_2$ . The loss on ignition S is

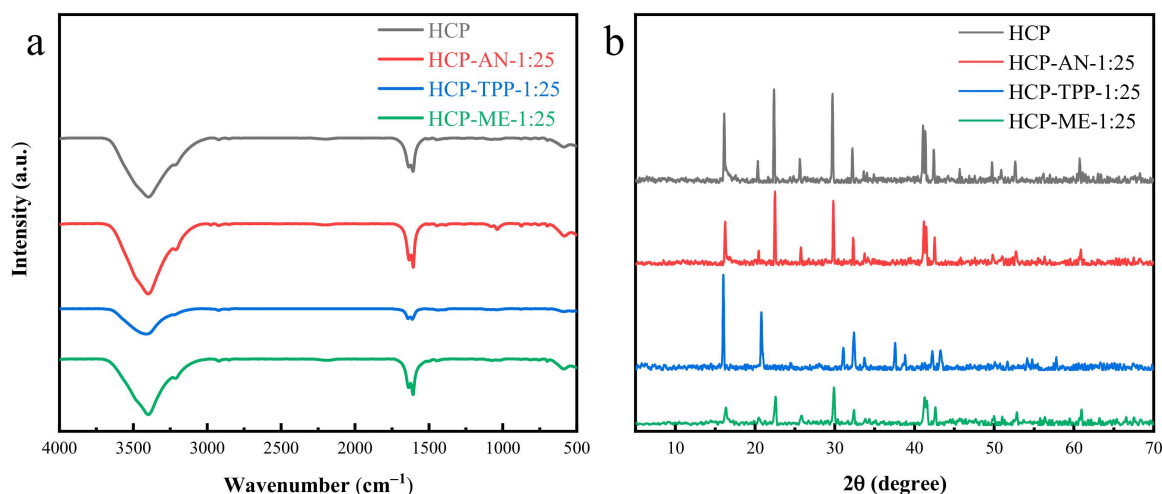
$$S = \frac{m_1 - m_2}{m_1 - m_0} \times 100\%$$

### 3. Results and Discussion

#### 3.1. Properties of HCP

The effects of additives on the performance of the products can be concluded from their characterization and analysis.

As shown in Figure 2a, the structure of the obtained HCPs was first characterized using an ATR-FTIR spectrometer. In the spectra, the peaks at  $1635\text{ cm}^{-1}$ ,  $1608\text{ cm}^{-1}$ , and  $1450\text{ cm}^{-1}$  can be attributed to the characteristic stretching vibration of the polystyrene phenyl skeleton, while the peaks at  $1700\text{--}2000\text{ cm}^{-1}$  indicate that the benzene ring is mono-substituted, and the peaks at  $2850\text{ cm}^{-1}$  and  $2920\text{ cm}^{-1}$  are attributed to  $-\text{CH}_2$  asymmetric stretching vibration and symmetric stretching vibration, respectively [43]. With the addition of the flame-retardant additives AN and ME, the absorption bands near  $3440\text{ cm}^{-1}$  and  $1450\text{ cm}^{-1}$  were enhanced, corresponding to the N-H stretching vibration and C-N vibration, respectively. This indicated that AN and ME were successfully doped into the HCP backbone. The enhancement of the characteristic peaks at  $3440\text{ cm}^{-1}$  and  $1450\text{ cm}^{-1}$  of HCP-ME was smaller than that of the peaks of HCP-AN, implying that it was physically doped with HCP. Conversely, the characteristic peaks at  $3440\text{ cm}^{-1}$  and  $1450\text{ cm}^{-1}$  of HCP-TPP were greatly weakened, which indicates that TPP has successfully reacted.

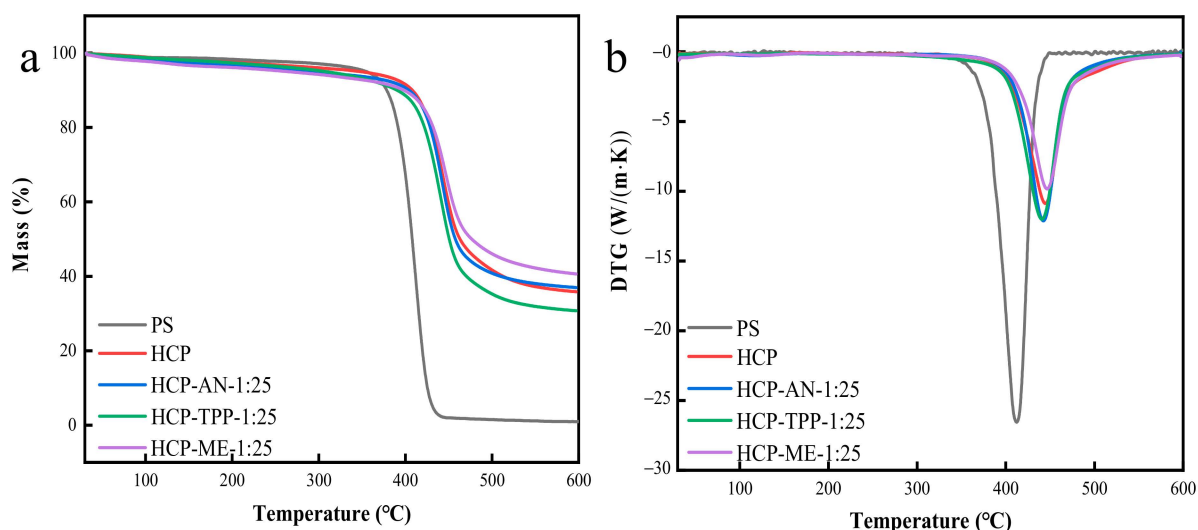


**Figure 2.** Characterization of HCP composite flame-retardant material. (a) FTIR image; (b) XRD image.

Afterward, the XRD spectra of the obtained samples were characterized. As shown in Figure 2b, it was found that the XRD diffraction profiles of the samples were similar due to the similar crystalline shape. The profiles of HCP-AN were weakened after  $45^\circ$ , whereas for HCP-TPP, new diffraction peaks were added near  $21^\circ$  and  $32^\circ$ . HCP and HCP-ME-1:25 showed similar XRD characteristic peaks; there was basically no change in the positions at which the diffraction peaks were located, and there were no obvious changes in the slit width of the diffraction peaks, which indicated that the addition of a small amount of ME would not change the crystal structure of the polystyrene composite flame-retardant material, and the change in the intensity of the diffraction peaks might be due to the slowing down of the nucleation rate caused by the addition of ME. It can be deduced that there are no chemical reactions in the preparation process with the addition of ME, but only physical and mechanical mixing.

Figure 3a,b show the TGA curves and derivative thermogravimetry (DTG) curves of HCP. The TGA curves of HCP show a clear one-step thermal decomposition process, which proceeds in three main stages. In the first stage, from  $30^\circ\text{C}$  to  $180^\circ\text{C}$ , the mass loss is mainly attributed to the volatilization of free and bound water and the decomposition of side chains in HCP [44]. In the second stage, from  $240^\circ\text{C}$  to  $320^\circ\text{C}$ , the main chain of HCP breaks down and decomposes to produce non-flammable gases [45]. The third stage is from  $320^\circ\text{C}$  to  $490^\circ\text{C}$  and is dominated by the continuous pyrolysis of HCP [46].

Table 2 shows the TGA test data of the samples under a nitrogen atmosphere. The analysis shows that the maximum loss rate of the HCP sample is  $-10.87\%/min$  at  $445\text{ }^{\circ}\text{C}$ , and the residual carbon content is  $35.85\text{ wt}\%$  at  $600\text{ }^{\circ}\text{C}$ , which is elevated by  $35\text{ wt}\%$  relative to pure PS, whose maximum loss rate is  $-26.54\%/min$  at  $413\text{ }^{\circ}\text{C}$ . Compared with HCP, HCP-AN-1:25 has  $36.96\text{ wt}\%$  residual carbon, but its thermal decomposition temperature starts earlier, with a maximum loss of  $-12.11\%/min$  at  $442\text{ }^{\circ}\text{C}$ , which is attributed to the influence of  $\text{NH}_3$  groups in HCP. In addition, the thermal stability of HCP-TPP-1:25 is reduced, with a residual carbon content of  $30.73\text{ wt}\%$ , and its thermal decomposition starts earlier than that of HCP, with a maximum loss rate of  $-12.00\%/min$  at  $441\text{ }^{\circ}\text{C}$ , whereas, for the sample physically doped with the ME flame retardant, the residual carbon content of HCP-ME-1:25 is  $40.63\text{ wt}\%$  at  $600\text{ }^{\circ}\text{C}$ , much higher than indicated in previous research on flame-retardant materials for PS [40,46,47], and the maximum loss rate is  $-9.81\%/min$  at  $446\text{ }^{\circ}\text{C}$ . The maximum loss rate is  $-9.81\%/min$ , but the weight loss at 1% and 5% occurs at a much lower temperature, which may be because the sample contains more moisture and has ME distributed on its surface, which is pyrolyzed in advance. It is important to note that a low thermal decomposition temperature does not mean low flame retardancy. The lower the decomposition temperature of the sample, the earlier it decomposes to produce a non-flammable gas/film, resulting in a flame-retardant effect.



**Figure 3.** Characterization of HCP composite flame-retardant material. (a) TGA image; (b) DTG image.

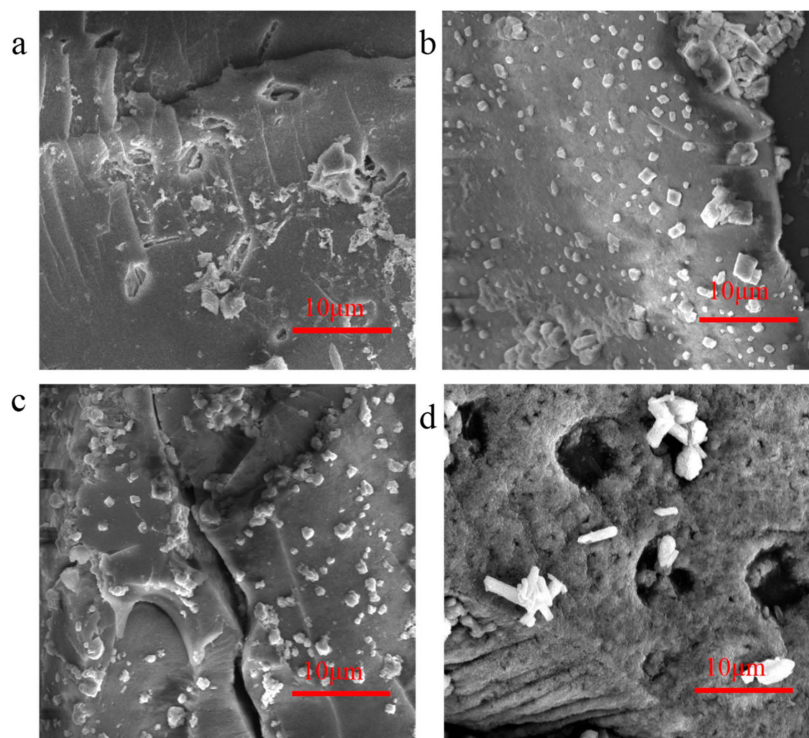
**Table 2.** TGA data for samples under a nitrogen atmosphere.

Sample	T <sub>1</sub> (°C)	T <sub>2</sub> (°C)	T <sub>3</sub> (°C)	T <sub>max</sub> (°C)	CR (wt%)
PS	88	355	378	413	0.95
HCP	95	348	408	445	35.85
HCP-AN-1:25	72	287	404	442	36.96
HCP-TPP-1:25	85	308	390	441	30.73
HCP-ME-1:25	46	264	398	446	40.63

T<sub>1</sub>: temperature at 1% loss of sample weight; T<sub>2</sub>: temperature at 5% loss of sample weight; T<sub>3</sub>: temperature at 10% loss of sample weight; T<sub>max</sub>: temperature of a maximum rate of degradation; and CR: char residue at  $600\text{ }^{\circ}\text{C}$ .

In Figure 4a–d, SEM images show the microscopic morphology of the samples. There are particles on the surface of the material, and there is a crosslinking phenomenon. In Figure 4a–c, it is observed that the surface of the sample is relatively rough and has a porous structure, and there are smaller particles of material distributed on the surface. The particles are the ferric chloride catalyst, and they are distributed on the surface of the material after the material is milled. This may help to improve its flame retardancy. Comparing Figure 4a–c, it can be observed that the microscopic morphology of HCP-ME is

quite different from the other three groups, with larger particulate matter distributed on its surface in Figure 4d, which is the reason that the ME molecules cannot participate in its reaction but are added to the material in the form of physical mixing, and thus, there are ME particles distributed on the surface of the material as well as in its interior. When the material burns, the ME molecules distributed on its surface will decompose and absorb heat, which improves the flame retardancy of the material.



**Figure 4.** SEM images of (a) HCP, (b) HCP-AN-1:25, (c) HCP-TPP-1:25, (d) HCP-ME-1:25.

### 3.2. Flame-Retardant Performance Test

To evaluate the material's flame-retardant properties, we conducted a loss-on-ignition test, which represents the amount of gaseous products released by the physical evaporation or chemical decomposition of raw materials due to heat [48,49].

Table 3 shows the loss-on-ignition data of the HCP flame-retardant materials, from which it can be seen that with the increase in AN addition, the loss on ignition of the materials decreases, and the loss on ignition was less than that of the control group without additives. From the loss-on-ignition test curve (Figure 5a), it was found that the mass of the samples changed a lot in the first 5 min, which is the main decomposition process. The mass curve for HCP-AN-1:10 stabilized at 14 min, HCP-AN-1:15 at 12 min, HCP-AN-1:20 at 16 min, and HCP-AN-1:25 at 22 min, indicating that the change in AN has a significant effect on its loss on ignition. This is because AN is an alkaline material and  $\text{FeCl}_3$  is an acidic catalyst; when too much of the flame-retardant additive AN is added, a mutual reaction between AN and  $\text{FeCl}_3$  occurs, which affects the structure of the product, so its loss on ignition increases and the curve stabilization time is prolonged. However, from the results of the loss on ignition, it can be seen that the loss on ignition of HCP-AN is smaller than that of HCP, which has a positive effect on the flame-retardant properties of the material. With the increase in TPP addition, the loss on ignition of the material increased. This may be attributed to the fact that TPP is a triphenyl structure containing multiple reaction sites, and the more TPP that is added, the less homogeneous the reaction is, leading to a decrease in the stability of HCP-TPP and an increase in the rate of loss on ignition. From the loss-on-ignition curve (Figure 5b), it was found that HCP-TPP has similar properties, and the main decomposition process occurs in the first 6 min; its final loss on ignition is

much smaller than that of HCP-AN, which is mainly because HCP samples doped with different flame-retardant additives had significantly different combustion products under aerobic conditions. Therefore, it is not appropriate to compare samples with different additives through loss on ignition, which should only be used to compare the same kinds of additives. The loss on ignition of HCP-ME did not show regular changes: HCP-ME-1:10 and HCP-ME-1:25 had a smaller loss on ignition, and HCP-ME-1:15 and HCP-ME-1:20 had a larger loss on ignition, the reason being the uneven distribution of ME molecules in the interior of HCP. However, it was found that the addition of ME reduced the burnout rate of HCP, which is because the addition of ME makes HCP-ME thermally decompose to produce ammonia and other gases, and ammonia decomposition is a kind of heat-absorbing reaction, as the resulting gas will take away heat in the form of thermal convection, which slows down the whole thermal decomposition process and reduces the rate of product loss on burning (Figure 5c).

Table 3. Loss on ignition of HCP samples.

Sample	S1	S2	S3	S4	S5	S6	S7
S (%)	0.44	0.34	0.38	0.39	0.46	0.25	0.24
Sample	S8	S9	S10	S11	S12	S13	
S (%)	0.20	0.19	0.28	0.36	0.35	0.29	

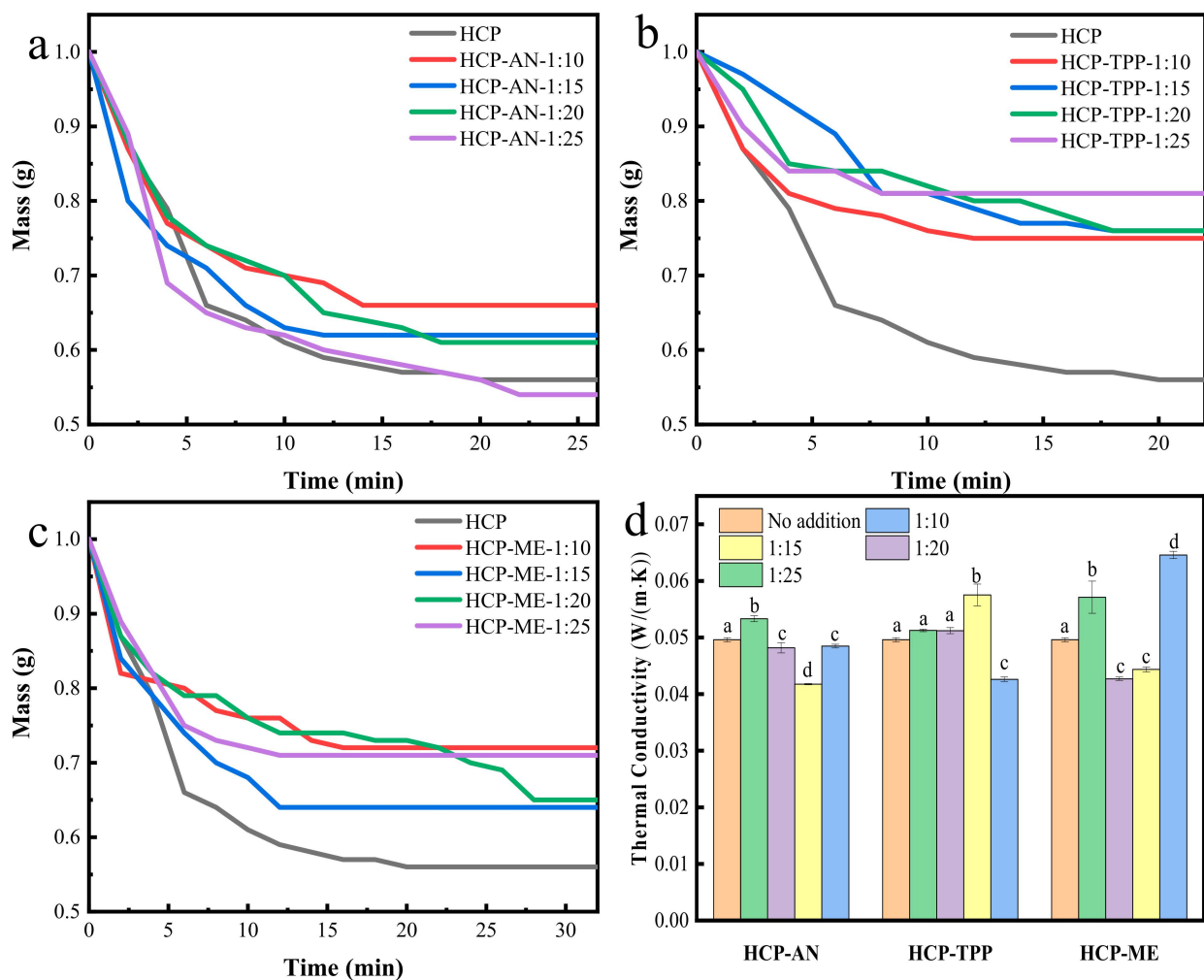
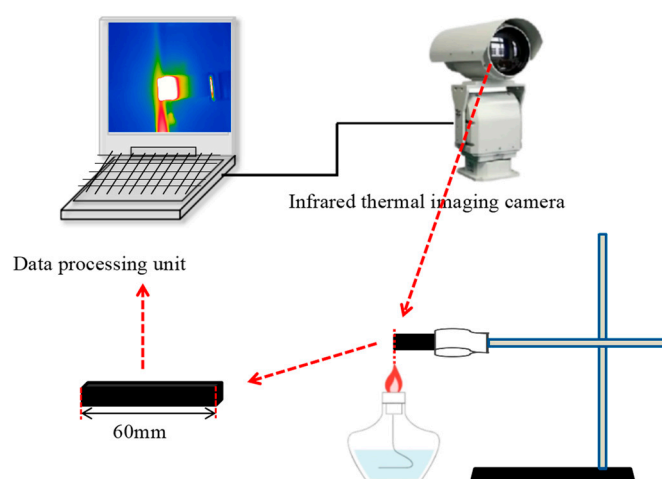


Figure 5. Flame-retardant test of HCP. (a) Mass change curve of HCP-AN, (b) mass change curve of HCP-TPP, (c) mass change curve of HCP-ME, (d) thermal conductivity test chart.



As shown in Figure 6, the PHCP sample (60 mm × 20 mm × 20 mm) was clamped to the iron frame table of the combustion test bench and burned with an alcohol lamp for 1 h. After that, the remaining length of the combusted sample was measured, and during this process, infrared thermal imaging cameras were used to observe the temperature distribution of the material during the combustion process. As can be seen from Table 4, the addition of the flame retardants AN, TPP, and ME has a positive effect on the flame retardancy of the materials. With the increase in the addition of the flame-retardant additive AN, the residual burning length of the PHCP-AN sample showed a gradual increase of 43 mm, 45 mm, 45 mm, and 47 mm, indicating that its flame-retardant effect increases with the increase in the molar fraction of flame-retardant additives. This is because of the presence of ammonium ions, so HCP-AN is thermally decomposed to produce ammonia, nitric oxide, and other non-combustible gases. Among them, ammonia will further decompose with oxygen and absorb heat. This process not only reduces the concentration of oxygen but also takes away the heat, so its flame-retardant properties are enhanced with the increase in the dosage of AN additives.



**Figure 6.** Combustion test experiment platform.

With the increase in the flame-retardant additive TPP, the residual burning length of the PHCP-TPP sample showed a gradual increase of 44 mm, 46 mm, 46 mm, and 47 mm, and the overall residual length was better than that of the PHCP-AN sample. As a kind of organic phosphorus flame retardant, the flame-retardant mechanism of TPP is as follows: HCP-TPP will decompose to generate metaphosphoric acid during the combustion process, and the metaphosphoric acid will polymerize to generate polymethyl metaphosphoric acid. In this process, the covering layer generated by phosphoric acid plays the role of a coating, but because the generated polymethylphosphoric acid is a strong acid with strong dehydrating properties, it will also make the polymer dehydrated and carbonized, change the combustion process of the polymer, and form a layer of carbon film on the surface of the polymer in order to insulate the air.

However, the residual burning lengths of HCP-ME did not change regularly with the increase in flame-retardant additives, and the overall residual burning lengths were 42 mm, 47 mm, 42 mm, and 48 mm with the increase in flame-retardant additives. The flame-retardant mechanism is similar to that of HCP-AN, but ME is doped into HCP in a physical form, which is different from the traditional means of physical doping, and this method leads to the uneven distribution of ME inside HCP, resulting in large changes in its flame-retardant effect. Therefore, in the future, the physical doping of flame retardants should focus on the doping method to ensure the uniform distribution of flame retardants.

It can be seen that, compared with the physical addition of the ME flame retardant, the chemical addition of the AN and TPP flame retardants is more stable in improving the flame-retardant performance of the material.

**Table 4.** Combustion test data.


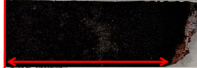


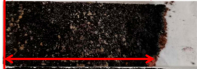






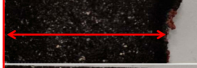

Sample	Burning Images	Residual Burning Length
S1		42 mm
S2		47 mm
S3		45 mm
S4		45 mm
S5		43 mm
S6		47 mm
S7		46 mm
S8		46 mm
S9		44 mm
S10		48 mm
S11		42 mm
S12		47 mm
S13		42 mm

Table 5 shows the infrared thermography of the sample combustion process. During the early stage of combustion (0~2 min), there will be a brief (<30 s) combustion phenomenon, and then the flame will extinguish on its own. From Table 4, it was found that during the entire heating process of the alcohol lamp, only the front part of the material is in a high-temperature state, while the back part is at room temperature, indicating that the material has an excellent insulation effect. However, during the flame combustion process, although the front part of the material does not self-ignite, a slow oxidation process occurs, causing the phenolic resin prepolymer of the material to lose its binding, become a powder, and fall off. In addition, it was found that the front end of the material can still maintain a high-temperature state after prolonged combustion. Only when the material burns to a sufficiently short state will the temperature at its front end return to normal, as shown in S11 and S13. Unfortunately, because the experimental process is susceptible to the influence of the external environment, we cannot compare and analyze the thermal insulation effect of the material from infrared thermography but only analyze the approximate pattern. Therefore, subsequent thermal conductivity testing of PHCP samples was carried out.

Table 5. Infrared thermal imaging data for combustion testing.

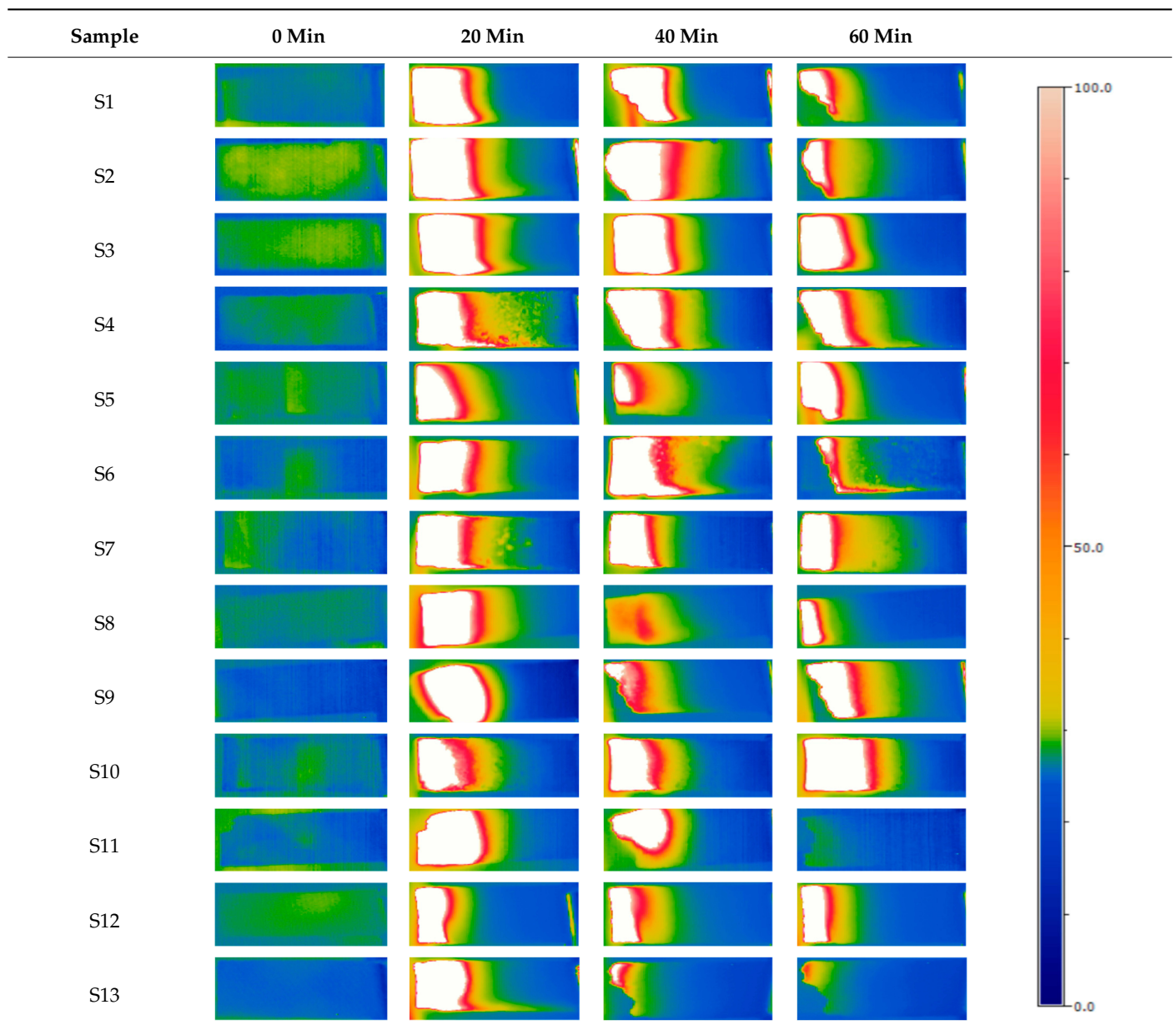


Figure 5d shows the thermal conductivity of the materials. In addition, Tukey’s test was performed on the obtained data and labeled a–d to indicate that there is a significant difference between the thermal conductivity of the samples, while the same labeled letters represent non-significant differences between the data. It was found that the samples all have low thermal conductivity, which indicates their excellent thermal insulation effect. For PHCP-AN, the thermal conductivity of PHCP increased with a small amount of AN, which may be attributed to the fact that too little AN has little effect on the pore structure of PHCP, and some impurities, such as FeCl<sub>3</sub>, remain in the pores of PHCP. With the increase in AN content, the thermal conductivity decreases and then increases. This is because when a small amount of AN, a flame-retardant additive, is added, the presence of AN increases the porosity of the product and raises its air sites, which increases its thermal resistance and enhances the thermal insulation effect of the samples. However, since AN is alkaline and FeCl<sub>3</sub> is an acidic catalyst, when too much of the flame-retardant additive AN is added, AN and FeCl<sub>3</sub> will react with each other, thus reducing the porosity of the product and weakening the heat insulation effect. For PHCP-TPP, a small amount of TPP addition does

not have a significant effect on its thermal conductivity, while when too much TPP is added, the thermal conductivity of PHCP-TPP first increases and then decreases, which is mainly related to the homogeneity of the TPP reaction; when the amount of TPP is increased, the homogeneity of the reaction deteriorates, which leads to a change in the structure of the product [43].

The thermal conductivity of PHCP-ME did not change regularly with the increase in the amount of ME added. Its thermal conductivity is mainly related to the distribution of ME; because PHCP is a porous material, when ME molecules are distributed inside the pores of the material, the pore diameter becomes smaller, the thermal resistance of materials is reduced, and the coefficient of thermal conductivity increases, which is especially obvious in S10, because S10 has more ME added. This also explains why S10 has the longest residual burning length in the combustion test, because ME is distributed inside the aperture of the material, which reduces the contact area of oxygen, on the one hand, and on the other hand, when the material burns, the flame retardant is distributed more widely and uniformly, which can better prevent combustion.

#### 4. Conclusions

In conclusion, this paper presents a simple method to prepare HCP with flame retardant and low thermal conductivity properties. HCP modified with different molar fractions of flame retardants was prepared from waste PS foam by selecting three flame-retardant additives, namely, AN, TPP, and ME. The process successfully doped the flame retardants into the porous structure of HCP by two methods, chemical reaction and physical mixing, to achieve the effect of in situ flame retardancy, after which the resulting materials were shaped with a phenolic resin prepolymer. The loss on ignition, combustion performance, and thermal conductivity of the materials were investigated with different ratios of flame-retardant additives to PS. It is worth noting that the method greatly improves the flame-retardant effect of the materials; the resulting materials all have enhanced flame-retardant properties, and the higher the amount of the flame-retardant additive added, the better the flame-retardant effect. Among them, HCP-ME-1: 10 has the best flame-retardant effect, and its remaining length (original length of 60 mm) can reach 48 mm after burning for 1 h. Compared with the physical addition of the ME flame retardant, the chemical addition of the AN and TPP flame retardants causes a more stable improvement in flame-retardant properties. It was found that the uniform distribution of the flame retardant inside the molecular pores of the material is the key to the improvement of molecular flame retardancy by physical addition. The results of thermal conductivity tests showed that the resulting materials all have excellent thermal insulation, with a minimum thermal conductivity of 0.04176 W/(m·K). This study successfully realized the conversion of waste polystyrene foam into flame-retardant materials, which provides a new idea for the high-value recycling of waste plastics and reduces their environmental pollution. This process not only reduces the dependence on primary fossil energy but also mitigates the negative impacts of waste plastics on the environment, which has certain application prospects in the field of building energy efficiency. Future research will focus on exploring the synergistic in situ flame retardancy of multiple flame retardants and their mechanisms in order to further enhance the high-value utilization of waste plastics and the potential for a wide range of applications.

**Author Contributions:** Conceptualization, C.L. and Z.W.; methodology, C.L.; formal analysis, Z.W.; investigation, C.L.; resources, C.L.; data curation, L.G.; writing—original draft preparation, Z.W.; writing—review and editing, Z.W., L.G., J.Z., W.Q. and C.L.; supervision, L.G., J.Z., W.Q. and C.L.; project administration, C.L.; funding acquisition, C.L. All authors have read and agreed to the published version of the manuscript.

**Funding:** The work is supported by the Fundamental Research Funds for the Central Universities (No. 2023ZDPY12). The authors also thank Dr. Hua Wei and Dr. Rui Zhou at Advanced Analysis & Computation Center of CUMT for their assistance with chemical analysis.

**Data Availability Statement:** The authors confirm that the data supporting the findings of this study are available within the article.

**Conflicts of Interest:** The authors declare that they have no known competing financial interests or personal relationships that could have appeared to influence the work reported in this paper.

### Abbreviations

AN	Aniline
DCE	1,2-Dichloroethane
DTG	Derivative thermogravimetry
FDA	Formaldehyde dimethyl acetal
FTIR	Fourier Transform Infrared Spectroscopy
GO	Graphene oxide
HCP	Hypercrosslinked polystyrene
IFR	Intumescent flame retardant
ME	Melamine
PRP	Phenolic resin prepolymer
PS	Waste polystyrene
PVC	Polyvinyl chloride
SEM	Scanning electron microscope
WBEP	Waterborne epoxy resin
XRD	X-ray polycrystalline diffractometer

### Nomenclature

CR	Char residue
$m_x$	Crucible mass
S	Loss on ignition rate
$T_f$	Weight loss temperature

### Subscripts

$f$	Loss
$x$	Factor

### References

- Dirksen, L.C. Plastic teeth: Their advantages and limitations. *J. Am. Dent. Assoc.* **1952**, *44*, 265–268. [[CrossRef](#)] [[PubMed](#)]
- Tang, G.; Qiao, W.; Wang, Z.; Liu, F.; He, L.; Liu, M.; Huang, W.; Wu, H.; Liu, H. Waste plastic to energy storage materials: A state-of-the-art review. *Green Chem.* **2023**, *25*, 3738–3766. [[CrossRef](#)]
- Thakur, S.; Verma, A.; Sharma, B.; Chaudhary, J.; Tamulevicius, S.; Thakur, V.K. Recent developments in recycling of polystyrene based plastics. *Curr. Opin. Green Sustain. Chem.* **2018**, *13*, 32–38. [[CrossRef](#)]
- Pathak, P.; Sharma, S.; Ramakrishna, S. Circular transformation in plastic management lessens the carbon footprint of the plastic industry. *Mater. Today Sustain.* **2023**, *22*, 100365. [[CrossRef](#)]
- Almeshal, I.; Tayeh, B.A.; Alyousef, R.; Alabduljabbar, H.; Mohamed, A.M.; Alaskar, A. Use of recycled plastic as fine aggregate in cementitious composites: A review. *Constr. Build. Mater.* **2020**, *253*, 119146. [[CrossRef](#)]
- Kim, S.; Kong, D.; Zheng, X.; Park, J.H. Upcycling plastic wastes into value-added products via electrocatalysis and photoelectrocatalysis. *J. Energy Chem.* **2024**, *91*, 522–541. [[CrossRef](#)]
- Zhao, C.; Liu, M.; Du, H.; Gong, Y. The Evolutionary Trend and Impact of Global Plastic Waste Trade Network. *Sustainability* **2021**, *13*, 3662. [[CrossRef](#)]
- Damayanti, D.; Saputri, D.R.; Marpaung, D.S.S.; Yusupandi, F.; Sanjaya, A.; Simbolon, Y.M.; Asmarani, W.; Ulfa, M.; Wu, H.-S. Current Prospects for Plastic Waste Treatment. *Polymers* **2022**, *14*, 3133. [[CrossRef](#)] [[PubMed](#)]
- Gao, C.; Huo, S.; Cao, Z. Solid Wastes Toward Flame Retardants for Polymeric Materials: A Review. *Front. Mater.* **2021**, *8*, 712188. [[CrossRef](#)]
- Delva, L.; Hubo, S.; Cardon, L.; Ragaert, K. On the role of flame retardants in mechanical recycling of solid plastic waste. *Waste Manag.* **2018**, *82*, 198–206. [[CrossRef](#)]
- Gomez, M.; Ernesto Peisino, L.; Kreiker, J.; Gaggino, R.; Cappelletti, A.L.; Martin, S.E.; Raggiotti, B.B. Stabilization of hazardous compounds from WEEE plastic: Development of a novel core-shell recycled plastic aggregate for use in building material. *Constr. Build. Mater.* **2020**, *230*, 116977. [[CrossRef](#)]
- Lucas, D.; Petty, S.M.; Keen, O.; Gaggino, R.; Cappelletti, A.L.; Martín, S.E.; Uberman, P.M.; Positieri, M.; Raggiotti, B.B. Methods of Responsibly Managing End-of-Life Foams and Plastics Containing Flame Retardants: Part II. *Environ. Eng. Sci.* **2018**, *35*, 588–602. [[CrossRef](#)]
- Troitzsch, J. Growing demand. *Kunststoffe-Plast Eur.* **2005**, *95*, 91–93.

14. Liang, S.; Neisius, N.M.; Gaan, S. Recent developments in flame retardant polymeric coatings. *Prog. Org. Coat.* **2013**, *76*, 1642–1665. [[CrossRef](#)]
15. Naiker, V.E.; Mestry, S.; Nirgude, T.; Gadgeel, A.; Mhaske, S.T. Recent developments in phosphorous-containing bio-based flame-retardant (FR) materials for coatings: An attentive review. *J. Coat. Technol. Res.* **2023**, *20*, 113–139. [[CrossRef](#)]
16. Li, S.; Wang, X.; Xu, M.; Liu, L.; Wang, W.; Gao, S.; Li, B. Effect of a biomass based waterborne fire retardant coating on the flame retardancy for wood. *Polym. Adv. Technol.* **2021**, *32*, 4805–4814. [[CrossRef](#)]
17. Liu, Q.; Wang, D.; Li, Z.; Li, Z.; Peng, X.; Liu, C.; Zhang, Y.; Zheng, P. Recent Developments in the Flame-Retardant System of Epoxy Resin. *Materials* **2020**, *13*, 2145. [[CrossRef](#)]
18. Dasari, A.; Yu, Z.-Z.; Cai, G.-P.; Mai, Y.-W. Recent developments in the fire retardancy of polymeric materials. *Prog. Polym. Sci.* **2013**, *38*, 1357–1387. [[CrossRef](#)]
19. Zhang, T.; Xie, H.; Xie, S.; Hu, A.; Liu, J.; Kang, J.; Hou, J.; Hao, Q.; Liu, H.; Ji, X. A Superior Two-Dimensional Phosphorus Flame Retardant: Few-Layer Black Phosphorus. *Molecules* **2023**, *28*, 5062. [[CrossRef](#)]
20. Luo, Y.; Geng, Z.; Zhang, W.; He, J.; Yang, R. Strategy for Constructing Phosphorus-Based Flame-Retarded Polyurethane Elastomers for Advanced Performance in Long-Term. *Polymers* **2023**, *15*, 3711. [[CrossRef](#)]
21. Daniel, Y.G.; Howell, B.A. Phosphorus flame retardants from isosorbide bis-acrylate. *Polym. Degrad. Stab.* **2018**, *156*, 14–21. [[CrossRef](#)]
22. Li, D.; Li, C.; Jiang, X.; Liu, T.; Zhao, L. Synergistic effects of intumescent flame retardant and nano-CaCO<sub>3</sub> on foamability and flame-retardant property of polypropylene composites foams. *J. Cell. Plast.* **2018**, *54*, 615–631.
23. Baochai, L.; Bakar, A.A.; Mohamad, Z. An overview of the recent advances in flame retarded poly(lactic acid). *Polym. Adv. Technol.* **2023**, *34*, 1435–1450. [[CrossRef](#)]
24. Birnbaum, L.S.; Staskal, D.F. Brominated flame retardants: Cause for concern? *Environ. Health Perspect.* **2004**, *112*, 9–17. [[CrossRef](#)] [[PubMed](#)]
25. Drehe, M.; Simulescu, V.; Ilia, G. Progress in the development of flame retardants. *Rev. Chem. Eng.* **2008**, *24*, 263–302.
26. Ilia, G.; Drehe, M. Grafted 2-chloroethylphosphonic acid on inorganic supports used as flame retardant for unsaturated polyester resins. *Fire Mater.* **2010**, *34*, 271–283. [[CrossRef](#)]
27. Zhang, C.; Jiang, Y.; Li, S.; Huang, Z.; Zhan, X.; Ma, N.; Tsai, F.C. Recent trends of phosphorus-containing flame retardants modified polypropylene composites processing. *Heliyon* **2022**, *8*, e11225. [[CrossRef](#)]
28. Li, L.; Wang, D.; Chen, S.; Zhang, Y.; Wu, Y.; Wang, N.; Chen, X.; Qin, J.; Zhang, K.; Wu, H. Effect of organic grafting expandable graphite on combustion behaviors and thermal stability of low-density polyethylene composites. *Polym. Compos.* **2020**, *41*, 719–728. [[CrossRef](#)]
29. Bhoite, S.P.; Kim, J.; Jo, W.; Bhoite, P.H.; Mali, S.S.; Park, K.-H.; Hong, C.-K. Expanded Polystyrene Beads Coated with Intumescent Flame Retardant Material to Achieve Fire Safety Standards. *Polymers* **2021**, *13*, 2662. [[CrossRef](#)]
30. Seidi, F.; Movahedifar, E.; Naderi, G.; Akbari, V.; Ducos, F.; Shamsi, R.; Vahabi, H.; Saeb, M.R. Flame Retardant Polypropylenes: A Review. *Polymers* **2020**, *12*, 1701. [[CrossRef](#)]
31. Luo, D.; Duan, W.; Liu, Y.; Chen, N.; Wang, Q. Melamine cyanurate surface treated by nylon of low molecular weight to prepare flame-retardant polyamide 66 with high flowability. *Fire Mater.* **2019**, *43*, 323–331. [[CrossRef](#)]
32. Zhao, Z.; Wang, X.; Wang, J.; Li, J. Study on preparation of highly dispersed graphite composite expandable polystyrene foam by homogeneous dissolution-suspension polymerization with waste polystyrene. *Polym. Eng. Sci.* **2022**, *62*, 1859–1866. [[CrossRef](#)]
33. Zhang, C.; Zhu, B.; Lee, L.J. Extrusion foaming of polystyrene/carbon particles using carbon dioxide and water as co-blowing agents. *Polymer* **2011**, *52*, 1847–1855. [[CrossRef](#)]
34. Li, M.-E.; Yan, Y.-W.; Zhao, H.-B.; Jian, R.-K.; Wang, Y.-Z. A facile and efficient flame-retardant and smoke-suppressant resin coating for expanded polystyrene foams. *Compos. Part B-Eng.* **2020**, *185*, 107797. [[CrossRef](#)]
35. Li, H.; Wang, X.; Yao, X.; Chu, H. Synthesis and properties of chlorine and phosphorus containing rubber seed oil as a second plasticizer for flame retardant polyvinyl chloride materials. *Pol. J. Chem. Technol.* **2023**, *25*, 36–42. [[CrossRef](#)]
36. Li, Z.; Li, W.; Liao, L.; Li, J.; Wu, T.; Ran, L.; Zhao, T.; Chen, B. Preparation and properties of polybutylene-terephthalate/graphene oxide in situ flame-retardant material. *J. Appl. Polym. Sci.* **2020**, *137*, e49214. [[CrossRef](#)]
37. Solis, R.R.; Gonzalez, M.D.C.; Blazquez, G.; Calero, M.; Martín-Lara, M.A. Activated char from the co-pyrolysis of polystyrene and olive stone mixtures for the adsorption of CO<sub>2</sub>. *J. Environ. Chem. Eng.* **2023**, *11*, 111370. [[CrossRef](#)]
38. Vijaya, S.; Kennedy, L.J. From waste to energy storage: Post-consumer waste expanded polystyrene/rGO composite as a high performance self-standing electrode for coin cell supercapacitors. *Rsc Adv.* **2024**, *14*, 689–699. [[CrossRef](#)]
39. Zhang, Y.; Wang, J.; Yang, X.; Ali, H.M.; Said, Z.; Liu, C. Fabrication of shape-stabilized phase change materials based on waste plastics for energy storage. *J. Energy Storage* **2022**, *52*, 104973. [[CrossRef](#)]
40. Kurt, A.; Ates, H. Effect of porosity on thermal conductivity of powder metal materials. *Mater. Des.* **2007**, *28*, 230–233. [[CrossRef](#)]
41. Liu, C.; Ma, X.; Du, P.; Rao, Z. Fabrication of highly efficient thermal energy storage composite from waste polystyrenes. *Chem. Eng. Sci.* **2020**, *216*, 115477. [[CrossRef](#)]
42. Liu, C.; Xie, Y.; Gao, D.; Shi, X.; Rao, Z. Fabrication of fire-retardant building materials via a hyper-crosslinking chemical conversion process from waste polystyrenes. *Energy Built Environ.* **2022**, *3*, 226–232. [[CrossRef](#)]
43. Liu, C.; Xiao, T.; Yang, X.; Wang, J.; Zhang, Y.; Said, Z. Comprehensive use of fossil derivative: High value-added conversion of waste plastics to thermal energy storage materials. *J. Energy Storage* **2023**, *73*, 108887. [[CrossRef](#)]

44. Han, D.; Zhao, H.; Gao, L.; Qin, Z.; Ma, J.; Han, Y.; Jiao, T. Preparation of carboxymethyl chitosan/phytic acid composite hydrogels for rapid dye adsorption in wastewater treatment. *Colloids Surf. a-Physicochem. Eng. Asp.* **2021**, *628*, 127355. [[CrossRef](#)]
45. Mohammadalizadeh, A.; Elmi, F. Flame retardant and superoleophilic polydopamine/chitosan-graft (g)-octanal coated polyurethane foam for separation oil/water mixtures. *Int. J. Biol. Macromol.* **2024**, *259*, 129237. [[CrossRef](#)] [[PubMed](#)]
46. Tang, W.; Huang, D.; Qiang, X.; Liu, W. Preparation of Hydrophilic and Fire-Resistant Phytic Acid/Chitosan/Polydopamine-Coated Expanded Polystyrene Particles by Using Coating Method. *Coatings* **2024**, *14*, 574. [[CrossRef](#)]
47. Baby, A.; Tretsiakova-McNally, S.; Joseph, P.; Zhang, J.; Arun, M. The Effects of Nitrogen-Containing Monomers on the Thermal Degradation and Combustion Attributes of Polystyrenes Chemically Modified With Phosphonate Groups. *Macromol. Mater. Eng.* **2024**, *309*, 2300432. [[CrossRef](#)]
48. Shi, L.; Chew, M.Y.L. Experimental study of woods under external heat flux by autoignition Ignition time and mass loss rate. *J. Therm. Anal. Calorim.* **2013**, *111*, 1399–1407. [[CrossRef](#)]
49. Beaudoin, A. A comparison of two methods for estimating the organic content of sediments. *J. Paleolimnol.* **2003**, *29*, 387–390. [[CrossRef](#)]

**Disclaimer/Publisher’s Note:** The statements, opinions and data contained in all publications are solely those of the individual author(s) and contributor(s) and not of MDPI and/or the editor(s). MDPI and/or the editor(s) disclaim responsibility for any injury to people or property resulting from any ideas, methods, instructions or products referred to in the content.